Experiments in Fluids 27 (1999) 522–532 © Springer-Verlag 1999

# Three-dimensional LDA measurements in the impeller region of a turbulently stirred tank

**J. J. Derksen, M. S. Doelman, H. E. A. Van den Akker**



**Abstract** Three-dimensional, angle-resolved LDA measurements of the turbulent flow field ($Re = 2.9 \times 10^4$) in the vicinity of a Rushton turbine in a baffled mixing tank have been performed. For this goal, a procedure for accurate beam alignment, based on a submerged micro-mirror system, has been developed. Results on the average flow field as well as on the complete set of Reynolds stresses are presented. The anisotropy of the turbulence has been characterized by the invariants of the anisotropy tensor. The trailing vortex structure, which is characteristic for the flow induced by a Rushton turbine, is demonstrated to be associated with strong, anisotropic turbulent activity.

**List of symbols**

| | |
|---|---|
| $a_{ij}$ | anisotropy tensor |
| $A_2$, $A_3$ | second and third invariant of the anisotropy tensor |
| $\|A\|$ | anisotropy parameter |
| $D$ | impeller diameter |
| $H$ | height of liquid level |
| $k$ | turbulent kinetic energy |
| $L$ | impeller blade length |
| $N$ | angular velocity (in rev/s) |
| $r$ | radial coordinate |
| $T$ | tank diameter |
| $\mathbf{u}$ | fluctuating velocity vector |
| $\mathbf{U}$ | instantaneous velocity vector |
| $v_{\mathrm{tip}}$ | impeller tip speed |
| $W$ | impeller blade height |
| $z$ | axial coordinate |
| $\alpha$ | element in the axisymmetric anisotropy tensor |
| $\delta$ | dimensionless deviation of the divergence from zero |
| $\delta_{ij}$ | unit tensor |
| $\Delta r$ | measurement grid spacing (radial direction) |
| $\Delta z$ | measurement grid spacing (axial direction) |
| $\lambda_i$ | $i$th eigenvalue of the anisotropy tensor |
| $\nu$ | kinematic viscosity |
| $\theta$ | tangential coordinate |
| $\Omega$ | angular velocity (in rad/s) |

**Superscript**

| | |
|---|---|
| — | time average |

*Received*: *14 September 1998 / Accepted*: *22 February 1999*

J. J. Derksen, M. S. Doelman, H. E. A. Van den Akker
Kramers Laboratorium voor FysischeTechnologie
Delft University of Technology
Prins Bernhardlaan 6
NL-2628 BW Delft; Netherlands

*Correspondence to*: J. J. Derksen

## 1 Introduction

Stirred tanks are encountered in a large variety of industrial processes. They are used for blending, for dispersing liquids, for bringing two (gas and liquid; liquid and solid) or three phases (gas, liquid and solid) into intimate contact, and, of course, as chemical reactors. Strict demands on product quality and environmental load ask for detailed process design, and, as a consequence, for a thorough understanding of the fluid dynamical aspects of turbulently operated stirred tanks. The role of experiments in this research area has shifted over the years. Characterization of the flow by means of global parameters, such as the power drawn by the impeller (see e.g. Rushton et al. 1950), the pumping capacity of the impeller, and the circulation times within the tank (Holmes et al. 1964), made way for local, mostly optical, flow measurements. A large amount of LDA data in stirred tanks of various configurations has been gathered (e.g. Wu and Patterson 1989; Yianneskis et al. 1987). Experimental data in the impeller outflow region have been extensively used as boundary conditions in steady-state flow simulations (Ranade and Joshi 1990; Bakker and Van den Akker 1994).

From a practical point of view, the flow at small scales is very important, as e.g. bubble or droplet break-up is controlled by the energy contained in eddies with sizes of the order of the bubble or droplet size. Also, the yield of chemical reactors can strongly depend on the way two or more components are brought into contact at the micro level (Bakker and Van den Akker 1996). At the same time, the smallest scales of the flow, along with the relevant quantities at these scales, such as the rate of energy dissipation, are still poorly accessible for experimental techniques. In a laboratory-scale tank, typically some 0.1 m in diameter operating at a typical Reynolds number between $10^4$ and $10^5$, the spatial resolution of an LDA measurement system can hardly reach the Kolmogorov length scale. A promising route to assess the small scales, which is becoming feasible with the availability of large computational resources, is to resolve (either directly or through closure, or

subgrid-scale models) the relevant local turbulence quantities by simulation (Eggels 1996; Derksen and Van den Akker 1998). The experimental data, necessary to validate these advanced simulations, have to meet high criteria in terms of accuracy and spatial resolution.

In this paper, we report on phase-resolved, three-dimensional LDA experiments in the impeller outflow region of a stirred tank at $Re = 2.9 \times 10^4$. The de facto standard geometry of a single Rushton turbine in a baffled tank was chosen. Phase-resolved LDA experiments in similar flow systems were reported by Yianneskis et al. (1987), Stoots and Calabrese (1995), Schäfer et al. (1996), and Lee and Yianneskis (1998) who all used 1D or 2D measurement systems. We explicitly made the choice for measuring the three velocity components simultaneously, because detailed experimental data on the complete Reynolds stress tensor, and, as a result, on the anisotropy of the turbulence are still lacking. For an unambiguous characterization of anisotropy, Reynolds *normal* stress data only are not sufficient. Kemoun et al. (1994) have reported results on all six components of the Reynolds stress tensor in the vicinity of a Rushton turbine. Their data are, however, not phase-resolved, and were obtained at $Re = 630$, i.e. in the transitional flow regime.

Additional advantages of a three-dimensional setup are in the fields of velocity bias correction and spatial resolution. In a three-dimensional setup, laser beam alignment is an important and difficult issue, especially when the working fluid has an index of refraction that strongly differs from its environment. An accurate alignment procedure, based on a submerged micro-mirror system, was developed for this goal.

The objective of the present study is to describe the structure of the (angle-resolved) turbulent flow field in the close vicinity of a Rushton turbine blade. The emphasis is on a high spatial resolution and on the characterization of the turbulence in terms of the Reynolds stress tensor, because these aspects are considered crucial for a critical evaluation of flow simulations. The small measurement volume of the three-dimensional setup, as well as the strict demands we have imposed upon coincidence of bursts at the three detector channels, lead to a relatively low data-rate, and therefore inhibit a characterization of the turbulence in terms of spectra. We do not feel this as a serious limitation, as the requirements for a meaningful interpretation of spectral information can hardly be met in stirred tank flow. In particular, the transformation of a temporal to a spatial spectral density requires the application of Taylor's hypothesis, which states that the speed at which a turbulence pattern moves past the measurement volume is closely equal to the mean velocity. It is obvious that this will only work if the mean velocity is large compared to the velocity scales of the turbulence (Bradshaw 1994). There may be no location within a stirred tank where this is the case. Michelet et al. (1997) experimentally explored in what way the convection velocity in the impeller stream of a stirred tank can be corrected to relate temporal and spatial fluctuations. The corrections they propose are quite severe.

## 2
## Flow geometry

The flow geometry is shown in Fig. 1. The baffled, flat-bottomed tank was filled with water up to a level

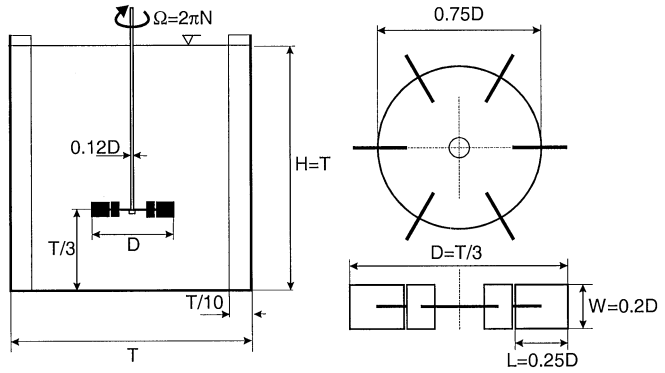


**Fig. 1.** The flow geometry. The tank (left) is equipped with four baffles to prevent solid body rotation of the fluid. The impeller (right) is a Rushton turbine. The diameter of the tank is $T = 288$ mm. The thickness of the disk and the impeller blades is 2 mm. The impeller was mounted on the shaft without a hub

$H = T = 288$ mm. At the top level there was a free surface. The Rushton turbine, with diameter $D = T/3$, was mounted with a bottom clearance equal to $T/3$. The cylindrical tank was entirely made out of high quality glass. To reduce refraction, it was placed in a square glass box filled with water as well. The impeller was set to revolve at an angular velocity of $N = \Omega/2\pi = 3.138(\pm 0.002)$ rev/s. Special care was taken in the fabrication of the impeller shaft. The eccentricity of the impeller motion was kept within 0.1 mm (i.e. 0.1% of the impeller diameter). The Reynolds number, which for this flow system is traditionally defined as $Re = ND^2/\nu$, amounted to $2.9 \times 10^4$ (at room temperature). The velocities in the tank will all be scaled with the impeller tip speed $v_{tip} = \pi ND$. The Froude number ($Fr = N^2D/g$, with $g$ the gravitational acceleration) was 0.1. It was observed that, under the conditions described above, the free surface was not distorted by air entrainment.

The way the impeller angle was measured was adopted from Stoots and Calabrese (1995). On the impeller shaft a phase encoder had been mounted. Every impeller revolution this encoder resets a 16 bit clock running at 10 kHz. Together with every valid LDA data point, two clock values were written to file: the time since the last clock reset, and the time of the last full impeller revolution. The ratio between these two times is a direct measure for the angle of the impeller at the actual velocity measurement. At the present impeller speed, the accuracy of this angle measurement is 0.15°.

## 3
## LDA setup

The sending optics of the LDA setup consisted of an Ar-ion laser, operating in all-lines mode, a beam splitter system (TSI Color Burst model 9201), and an optical fiber system that guided the beams to the flow. The ColorBurst selected the three major wavelengths of the laser and produced three pairs of beams. One beam of each pair was given a frequency pre-shift of 40 MHz. All beams were coupled into single-mode, polarization preserving optical fibers. They were coupled out in two laser probes. The initial spacing between the two beams in each pair was fixed to 50.0 mm. From probe #1 two beam pairs emerged. They were focused by a 500 mm lens, and entered the flow through the (flat) bottom of the tank (see Fig. 2). This

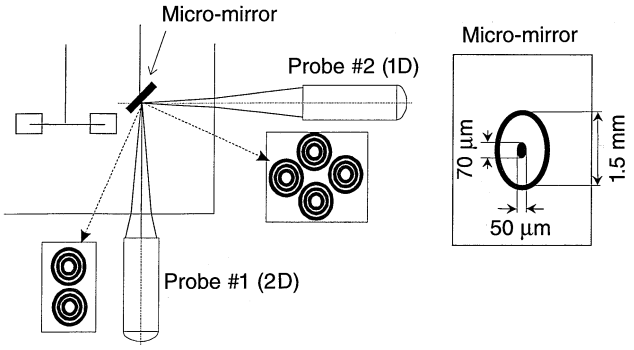


**Fig. 2.** The alignment system. Left: two fiber optic LDA probes were aligned with help of a micro-mirror. Right: dimensions of the micro-mirror. The outer elliptical ring-mirror was used to simplify finding the small mirror

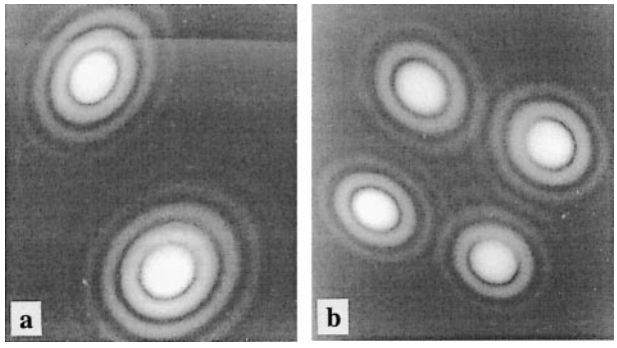


**Fig. 3.** **a** Diffraction pattern formed by the beams emerging from probe #2 when they are both optimally reflected by the micro-mirror. **b** The same as figure **a**, but now for the four beams emerging from probe #1

probe allowed for measuring the radial and tangential velocity component. The axial velocity component was measured with the single beam pair emerging from probe #2, which entered the vessel through the side-wall. This probe was equipped with a 250 mm front lens. If all beams show maximum overlap, a three-dimensional measurement volume of approximately $100^3$ µm$^3$ has been created.

The two probes contained the receiving optics as well. Lens systems in the probes projected the measurement volumes onto flat, multi-mode fiber-ends. These fibers guided the scattered light to three photo-multiplier tubes (one for each wavelength). An IFA 750 signal analyzer processed the photo-multiplier signals. The LDA system was operated in a (orthogonal) side scatter mode, i.e. light scattered by particles that traverse a measurement volume defined by the beams emerging from probe #1 was detected by probe #2, and vice versa. In order to increase scattered light levels, it was considered to build a non-orthogonal LDA setup (i.e. to place the optical axes of the two probes under an angle smaller than 90°). This option was rejected due to the construction of the LDA probes that only allowed for limited flexibility in manipulation of the individual beams. As a result of the latter, it was very difficult in a non-orthogonal layout to have the positions of the beam waists coinciding with the measurement volume.

The flow was seeded with aluminum coated polystyrene particles with a mean diameter of 4 µm. They were chosen because of their good light scattering properties. A disadvantage of these particles is their relatively high density ($2.6 \times 10^3$ kg/m$^3$) which forced us to keep the impeller running during the course of the experiments to prevent sedimentation.

### 3.1 Beam alignment

The entire flow system was placed in a three-dimensional traversing rig. The location of the measurement position could be defined (within a 0.1 mm accuracy) by traversing the tank and impeller relative to probe #2. This probe was fixed with respect to a laboratory frame of reference. Probe #1 was attached to an independent, three-dimensional traversing unit (accuracy 0.01 mm). It had to be positioned in such a way that maximum overlap of all three measurement volumes was reached.

The overlap was controlled and checked by means of an aluminum micro-mirror with elliptical shape (long axis: 70 µm, short axis: 50 µm) deposited on a sheet of glass (see Fig. 2). For reasons of protection, the aluminum was covered with a 500 nm quartz layer. The mirror was placed in the tank and then carefully traversed until the beams emerging from probe #2 showed (in reflection) a concentric diffraction pattern (as illustrated in Fig. 3a). Then, probe #1 was traversed until its four beams were optimally reflected by the micro-mirror as well (see Fig. 3b). After the mirror was retrieved from the vessel, an LDA measurement session could be started. The alignment procedure was repeated at every new measurement location in the vessel.

Figure 4 (the data rate in coincidence mode as a function of beam misalignment) gives an impression of the quality and resolution of the alignment system. A displacement in the *x*-direction (as defined in Fig. 4) obviously is most critical. A deviation of typically 10 µm from optimal alignment already causes a significant decrease of the coincident data rate. From a comparison between Figs. 4b and c, it can be concluded that the two-dimensional measurement volume (from probe #1) was about two times longer than the one-dimensional volume (from probe #2). This difference is related to the front lenses attached to the LDA probes, which had different focal lengths.

The IFA 750 signal processor uses the time stamps of burst validation to determine if a set of three Doppler bursts is coincident, i.e. falls within a pre-defined time window (the coincidence window). It was observed, however, that the location of the time stamp within a burst was not reproducible. Hence, in order to avoid the rejection of too many valid data, the coincidence window width was set to a significant fraction (about 50%) of the typical burst length at a specific measurement position. The window width varied between 0.5 and 1.0 ms, dependent on the location in the flow. The average inter arrival time on a *single* channel was at least two times larger than the coincidence window width. As a consequence, the influence of data points having false coincidence on the average flow field results is expected to be small.

### 3.2 Data processing

In the vicinity of the impeller tip, a measurement grid was defined in a vertical plane, midway between two baffles (see

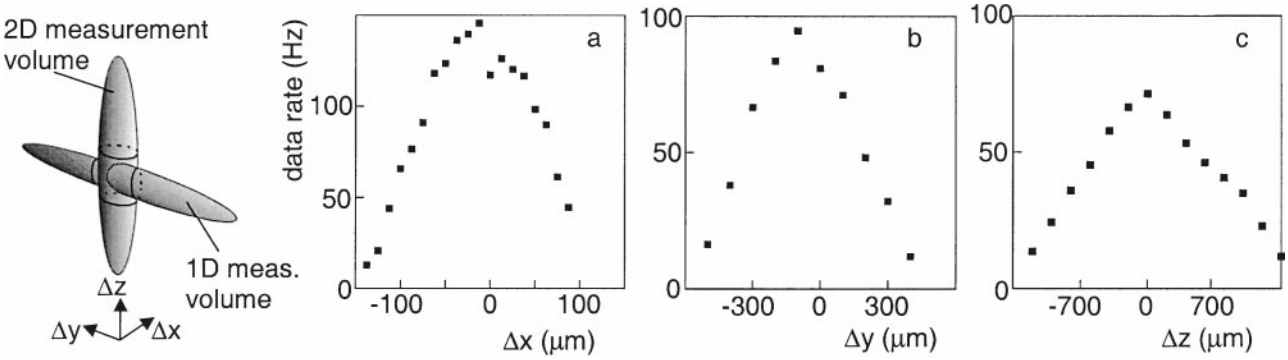


**Fig. 4.** The data rate in coincidence mode as a function of the position of the 2D measurement volume. The 2D measurement volume was traversed in the three directions defined in the left rendering. The origin of all three profiles was the position of optimal alignment ($\Delta x = \Delta y = \Delta z = 0$) as found with the micro-mirror system

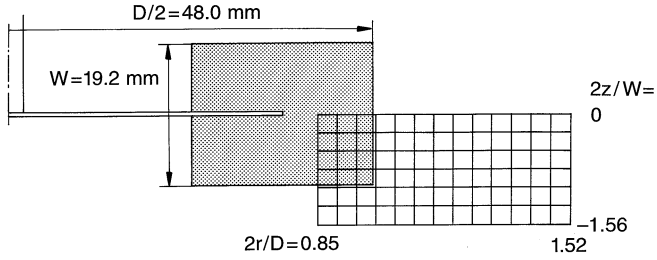


**Fig. 5.** The measurement grid was located in a vertical plane midway between two baffles. The grid spacing is $\Delta r = \Delta z = 2.5$ mm

Fig. 5). In Fig. 5, the coordinate system that will be used for presenting the flow field results is defined as well. The spacing of the grid in axial and radial direction was $\Delta z = \Delta r = 2.5$ mm, i.e. $\Delta z \approx W/8$ (with $W$ denoting the height of an impeller blade). In tangential direction, the resolution was 3° (at the inner bound of the grid this corresponds with a spacing of 2.2 mm, at the outer bound with 3.9 mm). Per grid point, i.e. per measurement position and tangential interval, $6 \times 10^3$ velocity samples were collected.

Velocity fluctuations in the flow region close to the impeller typically had an rms value of $0.25 v_{tip}$ (see also Sect. 4.2). As a result, the number of samples per average ensures a very small statistical uncertainity of the average velocities: about 0.5% of $v_{tip}$ (Benedict and Gould 1996). If statistical independence of the velocity samples is assumed, the standard deviation of the Reynolds stresses amounts to $10^{-3} v_{tip}^2$ (Benedict and Gould 1996). Reproducibility tests at the location $2z/W = 0.0$ and $2r/D = 0.94$ reveal deviations of $0.01 v_{tip}$ in the mean velocities, $0.02 v_{tip}$ in the rms values, and $0.002 v_{tip}^2$ in the shear stresses. These values are considered fair estimates of the accuracy of the presented data.

Burst-type LDA data in turbulent flows are inflicted by velocity bias: the particle transfer rate through the measurement volume is approximately proportional to the absolute value of the velocity. Therefore, unweighted averaging will lead to biased results. The average data presented in this paper were all corrected for velocity bias with velocity weighing, as introduced by McLaughlin and Tiederman (1973) (see also Gould and Loseke 1993), i.e. the moments $\overline{U_i^n\ U_j^m}$ were calculated according to

$$\overline{U_i^n\ U_j^m} = \frac{\sum_{k=1}^{M} U_{i,k}^n \cdot U_{j,k}^m \cdot 1/|\mathbf{U}|_k}{\sum_{k=1}^{M} 1/|\mathbf{U}|_k} \tag{3.1}$$

with $U_{i,k}$ denoting the $k$th measurement of velocity component $U_i$, $|\mathbf{U}|_k$ the absolute value of velocity sample $k$, and $M$ the total number of velocity samples. Note that the bias correction procedure explicitly uses the availability of all three velocity components in the same sample, as the inverse absolute velocity is the weighing factor. In the impeller outstream, the bias corrected mean tangential and radial velocity components were significantly smaller than their unweighted equivalents. The differences amounted up to $0.1 v_{tip}$.

## 4 Results

### 4.1 The average flow field

The structure of the average flow field, relative to an impeller blade (see Fig. 6). qualitatively corresponds with the results presented by Stoots and Calabrese (1995) and Lee and Yianneskis (1998). The wake behind an impeller blade can be clearly observed in Fig. 6a. In Lee and Yianneskis (1998) a vector plot at almost the same level in the tank is presented. Their wake is somewhat larger than the wake observed in Fig. 6a. Figure 6b shows the development of a strong three-dimensional vortex behind the impeller blade.

It is tempting to derive quantities such as the deformation rate (as done by Stoots and Calabrese 1995), or vorticity from the average field. However, only if the measurement grid is sufficiently fine, these operations are meaningful, because (discrete) spatial derivatives are involved. Calculation of the divergence of the flow field is a good check for the appropriateness of gradient operations in the measured flow field (Nieuwstadt 1997). In cylindrical coordinates, the divergence reads

$$\nabla \cdot \overline{\boldsymbol{U}} = \frac{1}{r}\frac{\partial}{\partial r}(r\overline{U_r}) + \frac{1}{r}\frac{\partial}{\partial \theta}\overline{U_\theta} + \frac{\partial}{\partial z}\overline{U_z} \tag{4.1}$$

In a grid that is sufficiently fine to capture all details of the average flow field, $\nabla \cdot \overline{\boldsymbol{U}}$ is zero (except for measurement errors).

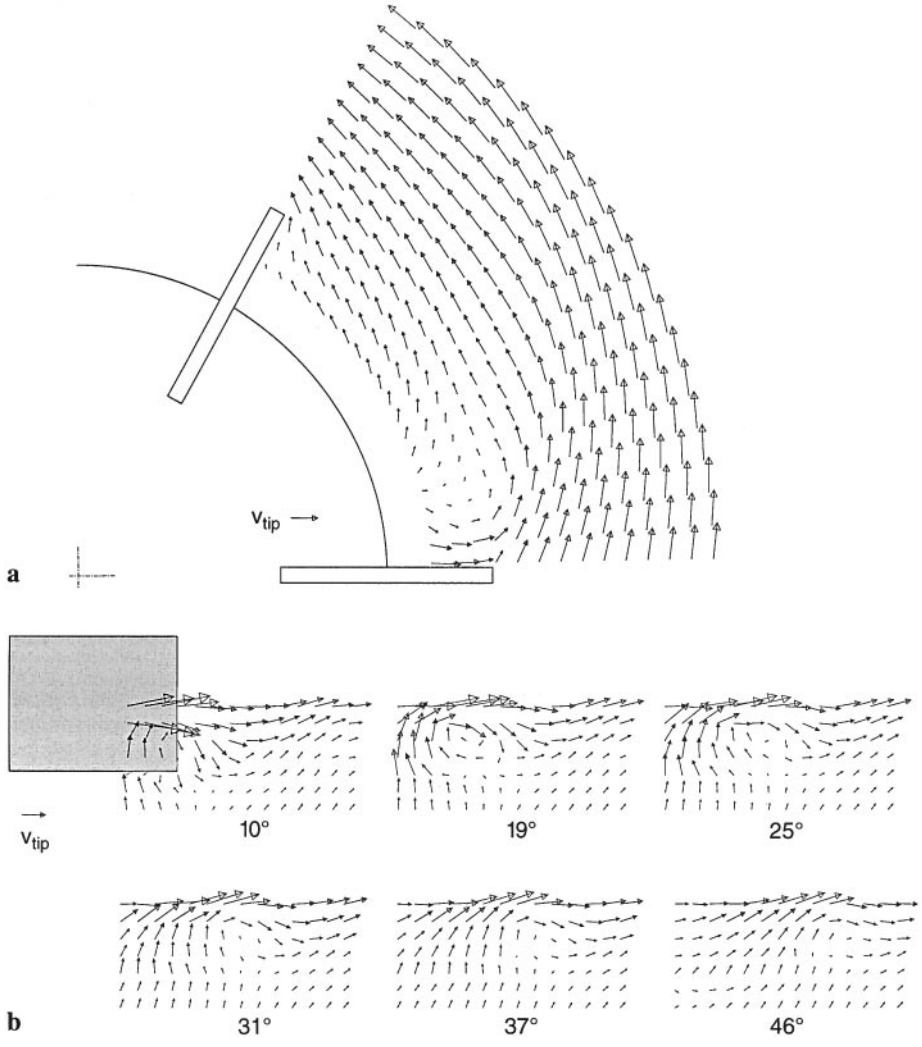


**Fig. 6. a, b**. The average flow field. **a** Velocity relative to the impeller in a horizontal plane at the level $2z/W = -0.52$; **b** velocity in six vertical planes at different angles with respect to the leading impeller blade

A parameter $\delta$, which is a non-dimensional measure for the deviation of the divergence from zero, was defined as:

$$\delta = \left| \frac{\nabla \cdot \overline{\boldsymbol{U}}}{v_{\text{tip}}/L} \right| \tag{4.2}$$

The gradients involved were calculated using a central differencing scheme. Consequently, the divergence was determined at locations exactly in the center of a control volume defined by the eight grid points at its corners. The gradients were non-dimensionalized by $v_{\text{tip}}/L$, with $L$ the length of an impeller blade (see Fig. 1). The measurement error we make when calculating the divergence is mainly due to the imprecision in the position of the measurement volume, which was about 0.1 mm (i.e. 4% of the grid spacing). As a result, the absolute error in $\delta$ was estimated to be 1.0.

Figure 7 shows the distribution of $\delta$ in a set of vertical planes with different angles with respect to an impeller blade. In the close vicinity of an impeller blade, $\delta$ is significantly higher than 1.0. Apparently, the boundary layers that are present at the blade surface cannot be fully resolved by our measurement grid. This observation has a direct consequence for *simulations* of the flow field. The resolution of a CFD simulation, either a direct simulation or a simulation employing some sort of turbulence modeling, has to be such that it is capable of adequately resolving the *average* flow field. Our results show that a grid with typically eight nodes (or less) over the height of an impeller blade (as e.g. has been used by Jaworki et al. (1997) in their sliding mesh simulations) is definitely not capable of doing this correctly.

In spite of the locally insufficient grid resolution, the vorticity field was calculated with the same central differencing scheme as was used for the divergence. The vorticity vectors in a horizontal plane, just below the impeller disk are presented in Fig. 8. The trailing vortex, as observed in Fig. 6b, can be clearly identified as a region of concentrated vorticity. Note that at the lower right corner of the vector field the vortex from the preceding blade can still be distinguished.

Yianneskis et al. (1987) proposed to charaterize the curve along which the trailing vortex is swept into the tank by connecting the points in a horizontal plane with a mean axial velocity component equal to zero. In Fig. 9, the curves found in the literature (Yianneskis et al. 1987; Stoots and Calabrese 1995; Lee and Yianneskis 1998; Van't Riet and Smith 1975) are compared with the one deduced from the present flow field. The strong deviation between curve [1] and the other curves is commonly attributed to inertia of the relatively large particles

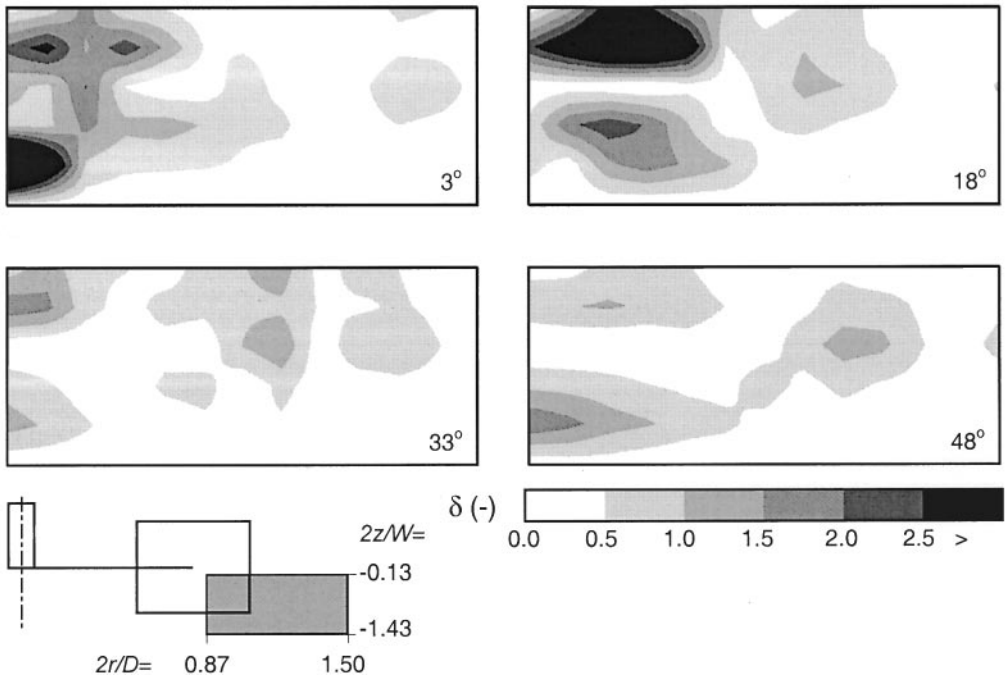


**Fig. 7.** The (dimensionless) divergence of the average flow field ($\delta$) as a function of the position in the tank. The parameter $\delta$ is defined in Eq. (4.2)

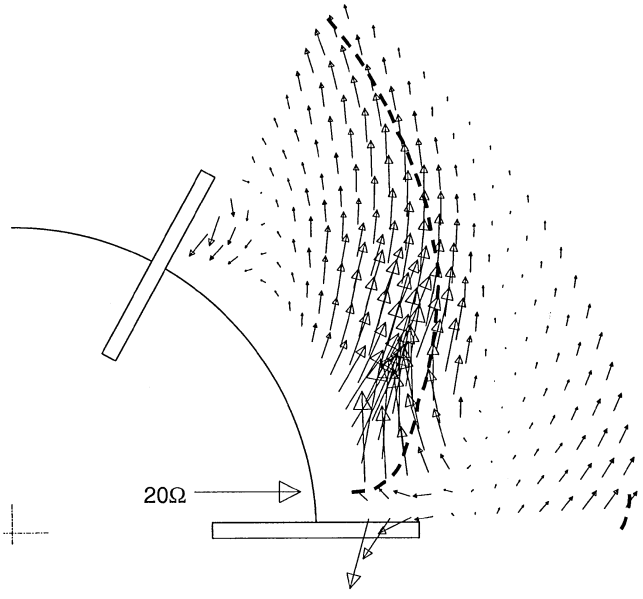


**Fig. 8.** The vorticity field in a horizontal plane at $2z/W = -0.39$. The vorticity is scaled with the angular velocity $\Omega(\Omega = 2\pi N)$. The dashed line is the position of the vortex core in the plane $2z/W = -0.52$

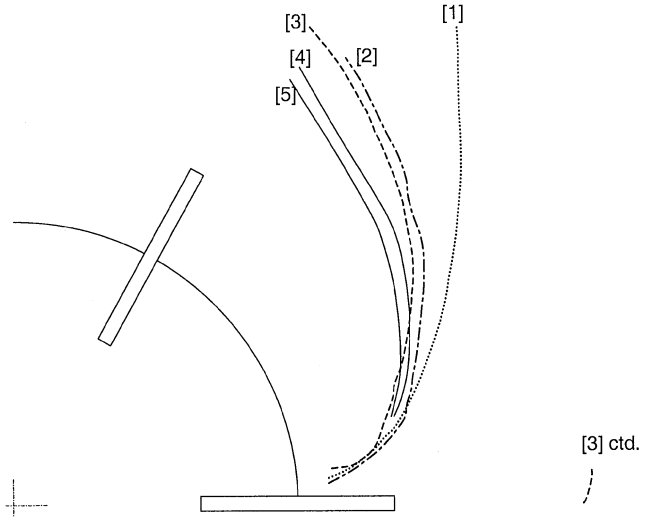


**Fig. 9.** The vortex core position deduced from several investigations reported in literature and from the present work. [1] Van 't Riet and Smith (1975); [2] Stoots and Calabrese (1995); [3] present work; [4] Yianneskis et al. (1987); [5] Lee and Yianneskis (1998)

(needed for a photographic technique) used by Van't Riet and Smith. We calculated, by linear interpolation, the position of zero axial velocity in the horizontal plane at a distance $2\Delta z$ below the impeller disk (i.e. at the $2z/W = -0.52$ level). According to Fig. 6b, this approximately was the plane in which the vortex core moved. Yianneskis et al. (1987) focused on the vortex shed from the upper part of the impeller blade. They claim that its core moved in the $2z/W = 1$ plane, which is in disagreement with our results if symmetry with respect to the plane of the disk is assumed (close to the impeller tip this seems a fair assumption, although the impeller was mounted with a bottom clearance $T/3$ in both studies). Stoots and Calabrese (1995) explicitly determined the vertical position of the lower vortex core. Close behind the impeller blade, the core was at $2z/W \approx -0.6$, while at larger angles with respect to the blade, the core moves towards $2z/W \approx -1$. Their impeller geometry, however, was quite different. Its disk had a diameter of $0.6D$, while in the present work it was $0.75D$; their bottom clearance was $T/2$. There is no statement on the vertical position of the vortex core in the study by Lee and Yianneskis

(1998). In the light of the discrepancies in the vertical position of the vortex core, it is clear that a rigorous comparison of the trajectories in a horizontal plane does not make much sense.

## 4.2 Turbulence characteristics



The major reasons for measuring Reynolds stresses can be found in the field of CFD. In the first place, the $k$–$\varepsilon$ model is still widely used for simulations in stirred tank configurations (e.g. Lundén 1995). Since this model is an eddy-viscosity model, it locally assumes isotropic turbulent transport. In rotating and/or highly three-dimensional flows, the $k$–$\varepsilon$ model is known to be inappropriate (Wilcox 1993). Assessment of the isotropy assumptions by experiment is therefore necessary. In the second place, a critical evaluation of simulations that actually predict Reynolds stresses (i.e. large eddy simulations and simulations employing higher-order closure models) requires experimental data.

First, the regions of high turbulent activity will be identified. This is done by plotting the turbulent kinetic energy $k=\frac{1}{2}\overline{u_i u_i}$ (with $u_i$ denoting the fluctuations about the mean of the $i$th velocity component, i.e. $U_i=\overline{U_i}+u_i$) as a function of the position (see Fig. 10). In the horizontal plane at $2z/W=-0.52$ it can be observed that the region with high turbulent activity more or less coincides with the trailing vortex path. The vertical sections through the flow field exhibit a concentrated region of high $k$ just above the vortex core. We speculate that this distribution of kinetic energy is (at least partly) due to random fluctuations in the vortex core position. Combined with the steep gradients in the flow field right above the vortex core (see Fig. 6b), erratic motion of the core position may locally lead to high levels of velocity fluctuations.

In order to give an idea of the levels of the Reynolds shear stresses, phase-averaged profiles are presented in Fig. 11. The data of the present study are compared to the data by Kemoun et al. (1994). The latter did not employ an angular resolved measurement system. As a result, apart from turbulent fluctuations, their stresses inherently contain the coherent fluctuations due to impeller blade passage. If we compare their total stresses with the ones deduced from the present study, a fair agreement can be observed. This is remarkable, given the large difference between the Reynolds numbers in both studies (630 versus $2.9\times10^4$).

We feel that a treatment in terms of (an)isotropy is beneficial for a meaningful interpretation of the Reynolds stresses. Therefore, in the remainder of this article the Reynolds stress data will be presented in terms of the anisotropy tensor $a_{ij}$ and its invariants (Lumley 1978). The anisotropy tensor, defined as

$$a_{ij}=\frac{\overline{u_i u_j}}{k}-\frac{2}{3}\delta_{ij} \tag{4.3}$$

has a first invariant equal to zero by definition. The second and third invariant respectively are $A_2=a_{ij}a_{ji}$ and $A_3=a_{ij}a_{jk}a_{ki}$. The range of physically allowed values of $A_2$ and $A_3$ is bounded in the $(A_3, A_2)$ plane by the so-called Lumley triangle (see Fig. 12). The boundary that appears to be most relevant in the current study is the boundary associated with axisymmetric turbulence.

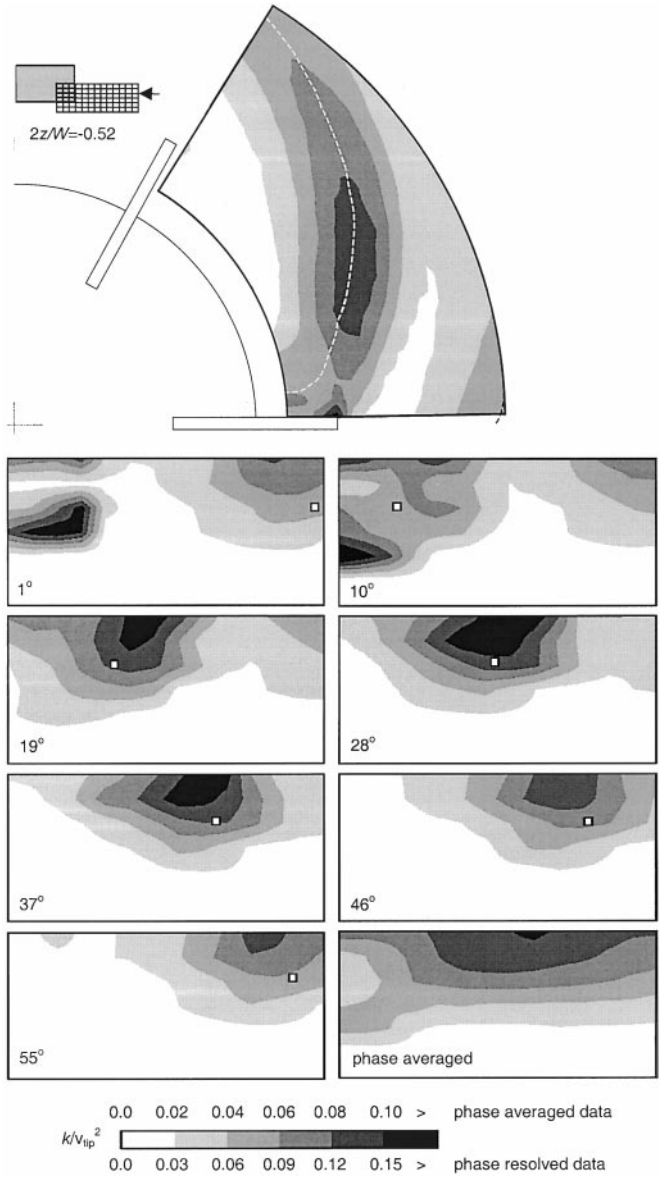


**Fig. 10.** The distribution of the turbulent kinetic energy $k=\frac{1}{2}\overline{u_i u_i}$ in the horizontal plane at $2z/W=-0.52$ (top figure); in seven $r$–$z$ planes with different angles with respect to the impeller blade; and in the $r$–$z$ plane averaged over all impeller angles. The vortex core position is indicated with a dashed line in the top figure. In the $r$–$z$ planes it is indicated with a small white square

In the case of axisymmetric turbulence, the kinetic energy in two orthogonal directions is equal. Hence, $a_{ij}$ can be written as

$$a_{ij}=\begin{pmatrix}-\alpha & 0 & 0\\ 0 & \alpha/2 & 0\\ 0 & 0 & \alpha/2\end{pmatrix} \tag{4.4}$$

in the principle coordinate system of tensor $a_{ij}$. The parameter $\alpha$ is related to the energy contained in the three coordinate directions. The energy contained in the first coordinate direction is $(\frac{1}{3}-\frac{1}{2}\alpha)k$. In this case, the invariants read $A_2=\frac{3}{2}\alpha^2$, and $A_3=-\frac{3}{4}\alpha^3$. Consequently, $A_3=6(A_2/6)^{3/2}$ if $\alpha<0$ (i.e. the energy contained in the symmetry direction exceeds $k/3$), and

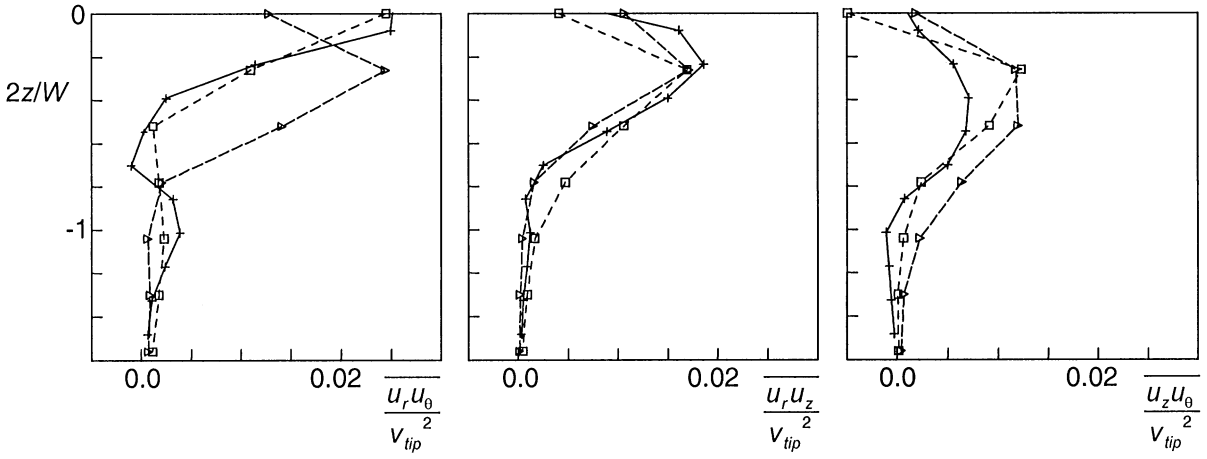


**Fig. 11.** Axial profiles of the phase-averaged Reynolds shear stresses. Total stress data by Kemoun et al. (1994) at $2r/D=1.15$ (denoted by $+$) are compared to the present results at $2r/D=1.16$ ($\triangle$ and $\square$). The $\triangle$ indicates stresses due to turbulent fluctuations only, whereas the $\square$ also contain the fluctuations due to impeller blade passage (i.e. total stress)

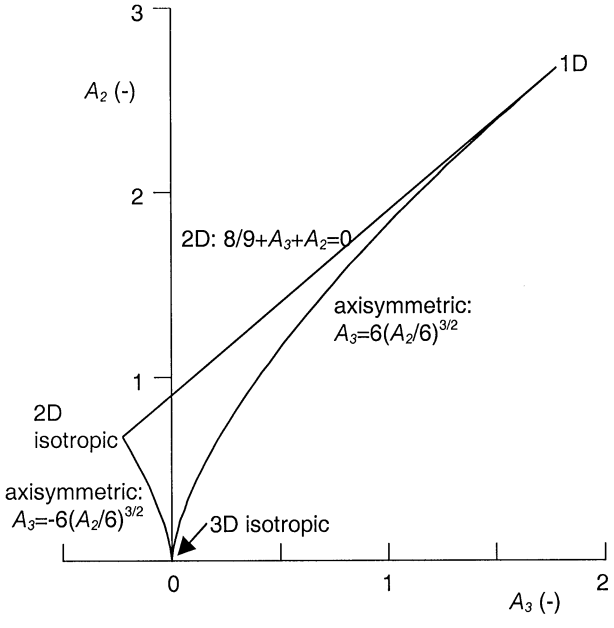


**Fig. 12.** The plane with coordinates $A_3$, $A_2$ (i.e. the invariants of the anisotropy tensor) was used to characterize the anisotropy of the turbulence. The physically possible states are bounded by the Lumley triangle (Lumley 1978)

$A_3=-6(A_2/6)^{3/2}$ if $\alpha>0$ (i.e. the energy contained in the symmetry direction is lower than $k/3$).

Most of the locations within the Lumley triangle, shown in Fig. 13, are close to the right, axisymmetric boundary of the Lumley triangle, which indicates that the most common situation in the present flow system is near-axisymmetric turbulence, with the energy contained in the direction of the axis of symmetry being highest. At the reference point on the axisymmetric curve, indicated in Fig. 13 with $\alpha=-1/3$, the turbulence is such that the energy contained in the symmetry direction is twice the energy in any of the two other directions. Many points in Fig. 13 are still further from isotropy than this reference point. In the near wake of the blade, at 4°, anisotropy is generally stronger than at larger angles.

In order to characterize anisotropy with a single parameter, the distance from the isotropic state $|A|=\sqrt{A_2^2+A_3^2}$ was defined. As a reference, the state with $\alpha=-1/3$ corresponds to $|A|=0.17$. Figure 14 shows that the strongest deviations from isotropy, i.e. the highest levels of $|A|$, occurred in the near wake of the impeller blades, at small lateral distances from the vortex core, and at the disk level in between the blades. In the plane $2z/W=-1.56$, the turbulence was almost isotropic.

To assess the direction of highest turbulent kinetic energy, the (orthogonal) eigensystems of the anisotropy tensors were determined. The energy contained in the direction of the $i$th eigenvector ($k_i$) is related to the $i$th eigenvalue of the anisotropy tensor ($\lambda_i$) according to

$$k_i=(\tfrac{1}{2}\lambda_i+\tfrac{1}{3})k \tag{4.5}$$

The direction of highest energy is confined primarily to the $r$–$z$ planes, as can be concluded from Fig. 15. Note that the vortex core is associated with an isotropic flow region. This could be due to fluctuations of the position of the vortex core. Combined with the steep velocity gradients in the $r$–$z$ plane, which are associated with the vortex structure, anisotropic velocity fluctuations may result. In Fig. 10, we have identified an intense turbulent region closely above the vortex core position. In the planes oriented 19° and 28° with respect to the impeller blade, the predominant direction of the turbulence in this region is radial. At larger angles, the direction shifts to axial, while, at the same time, the strength of anisotropy (in terms of $|A|$) decreases. Note the presence of an anisotropic region in the right part of the graphs at the 1° and 10° angles (Fig. 15). It is associated with the vortex that emerged from the previous impeller blade.

## 5
## Concluding remarks

Detailed studies on the flow field in a stirred tank ask for well-established experimental data on the average flow field,

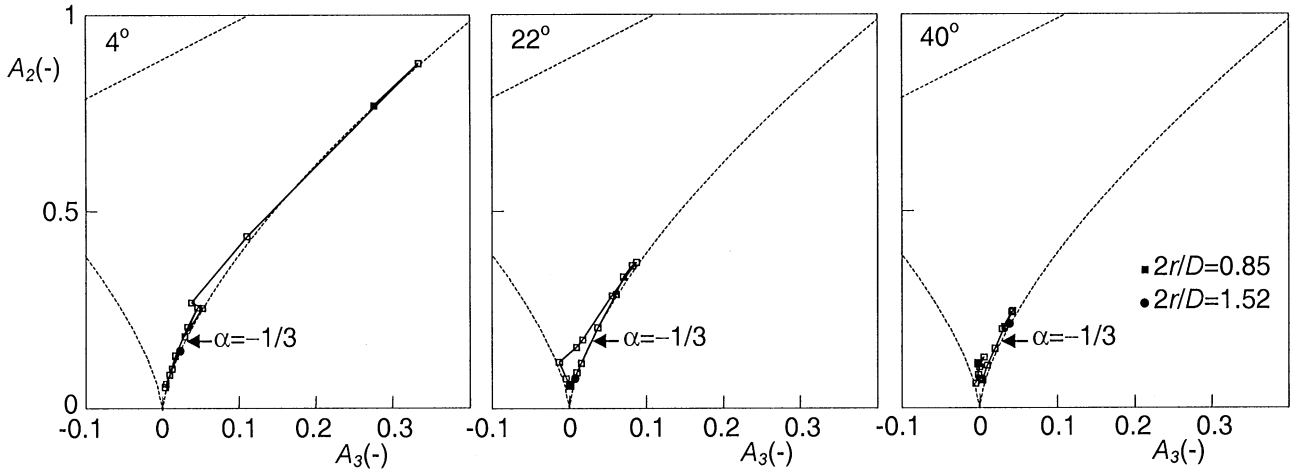


**Fig. 13.** The locations within the Lumley triangle along radially oriented lines in the flow field at the level $2z/W = -0.52$, and at three different angles with respect to an impeller blade. The starting point of a line is denoted with ■, the end point with ●. Most points are close to the right axisymmetric limit

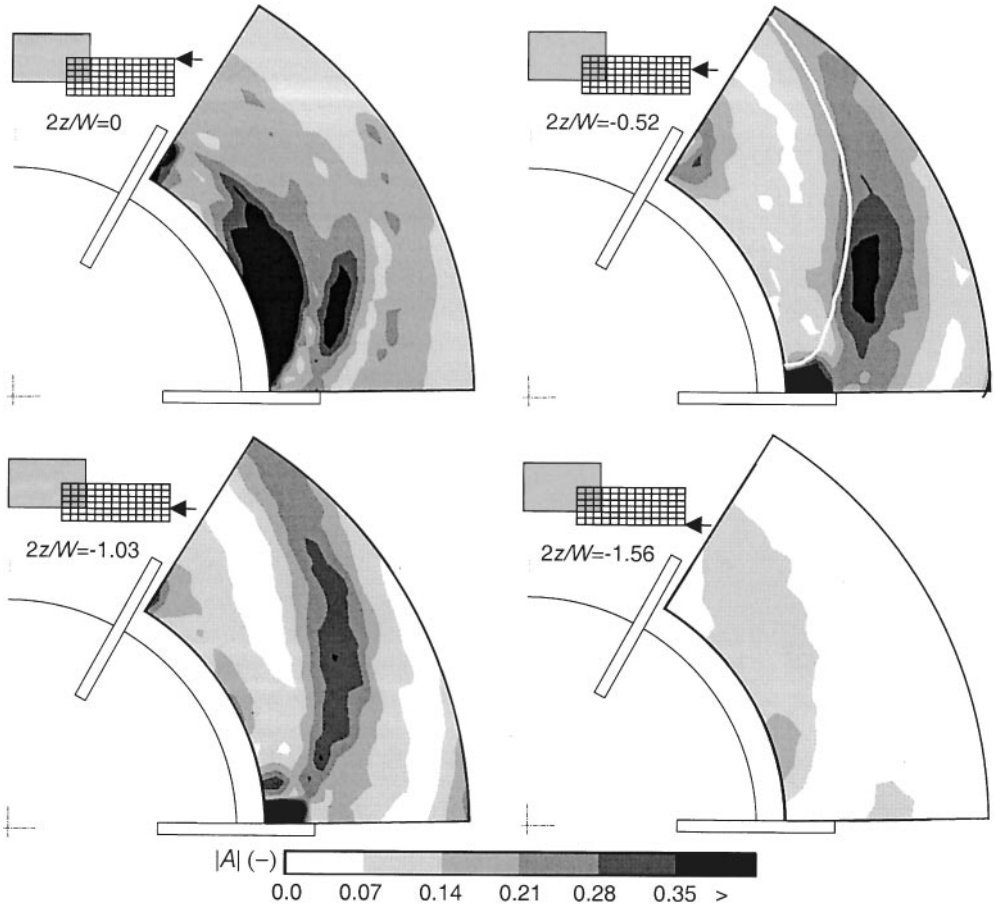


**Fig. 14.** The distribution of the aniosotropy parameter $|A| = \sqrt{A_2^2 + A_3^2}$ in a set of horizontal planes. The vortex core position is indicated in the plane $2z/W = -0.52$

and on the turbulence characteristics. Because of the three-dimensional character of the flow field, the experiment was chosen such as to measure the three velocity components simultaneously. This allowed for the characterization of the turbulence in terms of the (anisotropy of the) Reynolds stress tensor.

The experiments were carried out in a standard flow geometry, consisting of a baffled tank (diameter 288 mm) equipped with a Rushton turbine. The Reynolds number was $2.9 \times 10^4$. In order to align the two optical axes involved in the three-dimensional LDA setup, an alignment system, based on a submerged, elliptical micro-mirror ($50 \times 70$ μm$^2$), has been

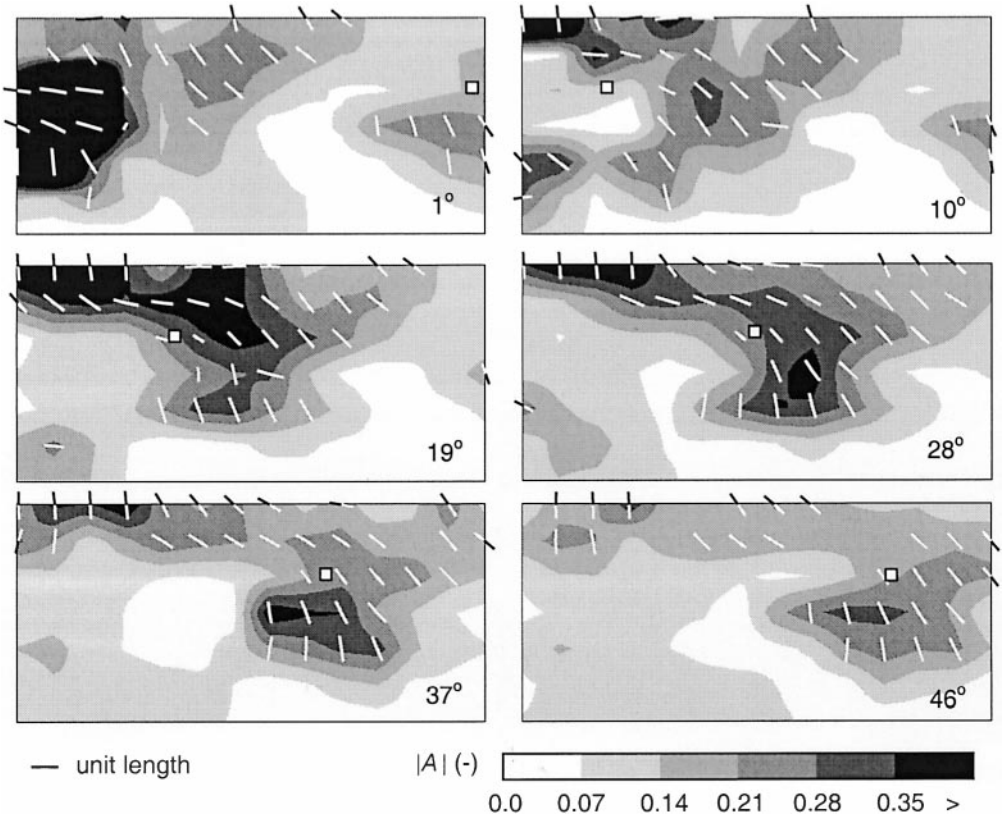


**Fig. 15.** The distribution of $|A|$ in six $r$–$z$ planes at different angles with respect to the impeller blade. The line pieces denote the orientation of the direction that contains the highest turbulent kinetic energy. Only if this direction contains at least half of the total amount of energy, the line piece is being depicted. All line pieces have unit length in three dimensions, i.e. the length in the $r$–$z$ plane is an inverse measure for the component in circumferential direction. The white squares denote the vortex core position

developed. Its resolution is of the order of 10 μm. Operation of the LDA system in side scatter mode resulted in a measurement volume with a linear dimension of approximately 0.1 mm in all three coordinate directions.

The averaged, phase-resolved flow field is characterized by a vortex that is developed in the wake of the impeller blade. This coherent structure could be clearly identified behind the blade over an angular range of more than 60°. As has been observed before (Lee and Yianneskis 1998), with the trailing vortex a region of high turbulent activity is associated. The strongest turbulent fluctuations were measured closely above the vortex core; this may be indicative of a significant contribution to the velocity fluctuations due to (random) vortex core motion.

The turbulence in several flow regions close to the impeller was demonstrated to be anisotropic. These regions are the near wake of an impeller blade, a region at disk level close to the disk, and the trailing vortex. The anisotropy in most points was nearly axisymmetric; i.e. the turbulent kinetic energy contained in two orthogonal directions was almost equal and significantly different from the energy in the third direction. The anisotropy near the trailing vortex decays when the vortex is swept into the bulk of the tank, while the orientation of the direction containing most of the kinetic energy is shifted from radial to axial.

As three-dimensional velocity information on a three-dimensional measurement grid was available, the divergence of the average flow field could be calculated. Closely behind an impeller blade, the divergence significantly deviated from zero, which indicates that in this region the spatial resolution of the measurement grid was insufficient to capture all details of the average flow field.

## References

**Bakker A; Van den Akker HEA** (1994) Single-phase flow in stirred reactors. Trans Int Chem Eng 72A: 583–593

**Bakker R; Van den Akker HEA** (1996) A Lagrangian description of micromixing in stirred tank reactors using 1D-micromixing models in a CFD flow field. Chem Eng Sci 51: 2643–2648

**Benedict LH; Gould RD** (1996) Uncertainty estimates for any turbulence statistics. 8th Int Symp on Applications of Laser Techniques to Fluid Mech. Lisbon: paper 36.1

**Bradshaw P** (1994) Turbulence: the chief outstanding difficulty of our subject. Exp Fluids 16: 203–216

**Derksen JJ; Van den Akker HEA** (1998) Parallel simulation of turbulent fluid flow in a mixing tank. Lect Notes Comput Sci 1401: 96–104

**Eggels JGM** (1996) Direct and large eddy simulation of turbulent fluid flow using the lattice-Boltzmann scheme. Int J Heat Fluid Flow 17: 307–323

**Gould RD; Loseke KW** (1993) A comparison of four velocity bias correction techniques for laser Doppler velocimetry. Trans ASME 115: 508–514

**Holmes DB; Voncken RM; Dekker JA** (1964) Fluid flow in turbine stirred, baffled tanks I: circulation time. Chem Eng Sci 19: 201–208

**Jaworski Z; Dyster KN; Moore IPT; Nienow AW; Wyszynski ML** (1997) The use of angle resolved LDA data to compare two differential turbulence models applied to sliding mesh CFD simulations in a stirred tank. Proc 9th European Conf on Mixing, pp 187–194

**Kemoun A; Lusseyran F; Mahouast M; Mallet J** (1994) Experimental determination of the complete Reynolds stress tensor in fluid agitated by a Rushton turbine. Int Chem Eng Symp Ser 136: 399–406

**Lee KC; Yianneskis M** (1998) Turbulence properties of the impeller stream of a Rushton turbine. AIChE J 44: 13–24
**Lumley J** (1978) Computational modeling of turbulent flows. Adv Appl Mech 26: 123–176
**Lundén M** (1995) Simulation of three-dimensional flow in stirred vessels. Influence of the impeller modeling and scale-up. Chem Eng Commun 139: 79–114
**Michelet S; Kemoun A; Mallet J; Mahouast M** (1997) Space-time correlations in the impeller stream of a Rushton turbine. Exp Fluids 23: 418–426
**McLaughlin DK; Tiederman WG** (1973) Bias correction methods for laser Doppler velocimeter counter processing. Phys Fluids 16: 2082–2088

**Nieuwstadt FTM** (1997) Private communication
**Ranade VV; Joshi JB** (1990) Flow generated by a disc turbine II. Trans Int Chem Eng 68: 34–50
**Rushton JH; Costich EW; Everett HJ** (1950) Power characteristics of mixing impeller I and II. Chem Eng Prog 46: 395–404 and 467–476
**Schäfer M; Höfken M; Durst F** (1996) Detailed LDV-measurements for visualization of the flow-field within a Rushton turbine. 8th Int Symp on Applications of Laser Techniques to Fluid Mech. Lisbon: paper 8.4
**Stoots CM; Calabrese RV** (1995) Mean velocity field relative to a Rushton turbine blade. AIChE J 41: 1–11
**Van't Riet K; Smith JM** (1975) The trailing vortex system produced by Rushton turbine agitators. Chem Eng Sci 30: 1093–1105
**Wilcox DC** (1993) Turbulence modeling for CFD, La Cañada (CA), DCW Industries
**Wu H; Patterson GK** (1989) Laser-Doppler measurements of turbulent-flow parameters in a stirred mixer. Chem Eng Sci 44; 2207–2221
**Yianneskis M; Popiolek Z; Whitelaw JH** (1987) An experimental study of the steady and unsteady flow characteristics of stirred reactors. J Fluid Mech 175: 537–555